Scanning Electrochemical Microscopy at Thermal Sprayed Anti-Corrosion Coatings: Effect of Thermal Spraying on Heterogeneous Electron Transfer Kinetics

Akbar Niaz,[a] *Adrian Boatwright,*[b] *K. T. Voisey*[a] *and Darren A. Walsh*[b,*]

[a]Faculty of Engineering and [b]School of Chemistry,

University of Nottingham,

Nottingham NG7 2RD, UK

Corresponding Author:

* darren.walsh@nottingham.ac.uk

Tel: +44 115 951 3437 Fax: +44 115 951 3562

ABSTRACT

The effect of thermal spraying on the electrochemical activity of an anti-corrosion superalloy was studied quantitatively using scanning electrochemical microscopy (SECM). The superalloy used was Inconel 625 (a Ni base superalloy) and thin coatings of this alloy were formed on mild steel using high velocity oxy-fuel (HVOF) thermal spraying. The kinetics of electron transfer (ET) across the Inconel 625 coating/electrolyte interface was studied using SECM employing ferrocenemethanol as the redox mediator. For comparison, the kinetics of ET across stainless steel/electrolyte and bulk wrought Inconel 625/electrolyte interfaces were also determined using SECM. The standard heterogeneous ET rate constant, k^0, for ferrocenemethanol reduction at stainless steel was $1.3\pm0.5\times10^{-4}$ cm s^{-1}, compared to $7.7\pm0.8\times10^{-4}$ cm s^{-1} at the wrought Inconel 625 surface. However, at the HVOF-sprayed Inconel 625 surface, the kinetics of ET varied across the surface and k^0 for ferrocenemethanol reduction ranged between $\sim2\times10^{-4}$ cm s^{-1} and $\sim5\times10^{-3}$ cm s^{-1}. These results clearly demonstrate that SECM can be used to quantify the effect of thermal spraying on the electrochemical properties of Inconel 625 and that thermal spraying results in an electrochemically-heterogeneous surface.

Keywords: Thermal spraying, electron transfer kinetics, ultramicroelectrode, superalloy

1. Introduction

Thermal-sprayed corrosion resistant coatings are used in a wide variety of industries to enhance the lifetime of engineering components [1]. A number of thermal spraying methods are available and include arc spraying, detonation gun spraying, low pressure plasma spraying and high velocity flame spraying [2]. The introduction of high velocity oxygen fuel (HVOF) spraying was one of the most significant developments in thermal spray technology and involves using a supersonic flame-jet to spray a feedstock powder through an expansion nozzle onto a substrate surface [3]. The jet accelerates and melts the powder particles, which upon impact with the substrate, deform and adhere by mechanical interlocking. HVOF processes use lower temperatures and higher velocities than other thermal spray processes, which results in more compact and better quality coatings than are obtained using many other thermal spray processes. A range of coatings have been formed using HVOF spraying, including metal carbide [4], cermet [5], ceramic [6] and polymer coatings [7].

One of the drawbacks of thermally sprayed coatings including HVOF coatings is that they do not offer the same level of corrosion resistance as the corresponding bulk alloys. Optimum coating performance is only achieved if the coating is free of interconnected pores and inclusions as these are potential sources of localized attack [8]. However, HVOF coating microstructures are dominated by inter-particle (splat) boundaries, which contain pores and inclusions that are often depleted of alloy elements [9]. As a result, the passivating films that form on these surfaces may not cover the metal surface uniformly resulting in less than optimum corrosion resistance. Therefore, visualization of the uniformity of the coating surface reactivity, as well as

measurement of the corrosion resistance of these coatings, is important for optimising their performance [10].

Scanning electrochemical microscopy (SECM) is an extremely powerful tool for obtaining spatially resolved reactivity information from surfaces. SECM is an electrochemical scanning probe technique that uses the faradaic reaction occurring between an ultramicroelectrode (UME) and a substrate surface as the analytical signal. The position of the UME (the SECM tip) is controlled using piezoelectric positioners and it can be moved perpendicular or parallel to the substrate to obtain information about the surface conductivity or reactivity [11]. SECM has been used to visualise the local electrochemical activity of materials such as iron [12], stainless steel [13, 14], anodized aluminium [15-19] and titanium oxide [20-22].

SECM was recently used to visualise the electrochemical activity of thin coatings of Inconel 625, a Ni base superalloy that is used as a corrosion-resistant material [23]. In this paper, we describe the use of SECM to quantify the effect of the HVOF process on the electron transfer (ET) reactivity of HVOF-sprayed Inconel 625. Furthermore, we compare the electrochemical activity of HVOF-sprayed Inconel 625 coating with that of a stainless steel substrate and a bulk wrought Inconel 625 substrate. SECM feedback approach curve experiments, in which ferrocenemethanol was used as a redox mediator, were used to determine the rate of ET across the interface between each substrate and an aqueous electrolyte. This analysis reveals that, in general, Inconel 625 is more electrochemically active than stainless steel. However, the HVOF process introduces heterogeneity to the surface of Inconel 625, which can be quantified by variations in the heterogeneous ET rate constant, k^0, when measured at different locations on the coating surface.

2. Experimental

2.1 Materials and Apparatus

Inconel 625 powder (particle size 20-53 μm) was obtained from William Rowland Ltd. (Sheffield, UK). Wrought Inconel 625 was from Special Metals Corporation (Hereford, UK) and mild and stainless steel substrates were from Smith Metals (Bedfordshire, UK). Thin coatings (approximately 300 μm thick) of Inconel 625 were formed on mild steel substrates using a Met-Jet II liquid fuel HVOF system (Metallization Limited, Dudley, UK) using the method described previously [23]. Pt wire (25 μm diameter) was from Goodfellow (Huntingdon, UK) and all chemicals were obtained from Sigma Aldrich and were used as received. Electrochemical experiments were performed using a Model 910B Scanning Electrochemical Microscope from CH Instruments Inc. (Austin, TX), a 12.5 μm radius Pt disk SECM tip (described below), an Ag|AgCl reference electrode and a Pt wire counter electrode. Electrolyte solutions were prepared using Milli-Q deionised water (18.2 MΩ).

2.2 Electrode Fabrication and Electrochemical Measurements

SECM tips were prepared by sealing 12.5 μm radius Pt wire in borosilicate glass and polishing the tip surface using the methods described previously [24]. The tip was

sharpened using a microelectrode beveller (Model BV-10 from Sutter Instruments, Novato, CA) to reduce the *RG* ratio of the tip ($RG = r_g/a$, where r_g is the radius of the insulating glass sheath and a is the Pt disk radius) to approximately 10. Prior to use, all substrates were polished using 1μm diamond polishing paste and, when required, electrical contact was made to the back of the substrate using copper wire. SECM experiments were performed by placing a drop of electrolyte (0.1 M K_2SO_4), containing 1 mM ferrocenemethanol (FcOH) as the redox mediator, onto the substrate surface. A Pt wire counter electrode and Ag| AgCl reference electrode were then placed into the drop of electrolyte and the SECM tip entered the drop from above.

2.3 Surface Profilometry and Scanning Electron Microscopy

Before conducting SECM experiments the surface profile of all samples was measured using a Talysurf CLI 1000-3D profilometer (Taylor Hobson Ltd., UK). An area of 5×5 mm was scanned using a 2 μm radius stylus at 500 μm s^{-1}. The average surface roughness was 0.043 μm, 0.048 μm and 0.068 μm for stainless steel, wrought Inconel 625 and the Inconel 625 coating, respectively. The surface of each material was characterised using a Phillips XL30 Scanning Electron Microscope. Prior to imaging by SEM, the substrate surfaces were etched to reveal microstructural features. The stainless steel and Inconel 625-coated steel sample were etched with 2% nital (2% nitric acid in ethanol) and wrought Inconel 625 was etched with aqua regia (1:3 concentrated HNO_3/concentrated HCl) for 10-15 seconds. The etched surfaces were then rinsed thoroughly with deionised water and dried in air.

3. Results and Discussion

3.1 Microstructural Examination of Inconel 625 Coatings

Figures 1A-1C shows SEM images of the surface of wrought Inconel 625 and the surface of the HVOF-sprayed Inconel 625 on mild steel substrates. The wrought alloy (Figure 1A) consists of single face-centred cubic (fcc) γ-phase solid solution with Mo and Nb rich carbides at the grain boundaries [25, 26]. Figure 1 shows that the surface morphology of the coated sample (Figure 1B) was very different from that of the wrought alloy. Approximately disk-shaped splats (black arrow in Figure 1B) were observed on the surface of the coated sample, as is common for HVOF-sprayed coatings of this material [23]. The black areas in Figure 1B are the splat boundaries (white arrow). During the HVOF process some oxidation of the hot alloy particles occurs, which depletes the outer regions of the particles of chromium and this depleted and oxidised material is predominantly found at the splat boundaries. It has been proposed that process-induced oxidation results in relatively poor corrosion resistance of the resulting coating [27].

3.2 Cyclic Voltammetry at Pt, Inconel 625 and stainless steel

Figure 2 shows cyclic voltammograms recorded at a range of scan rates in 1 mM FcOH at Pt, wrought Inconel 625, HVOF-sprayed Inconel 625 and stainless steel substrates. At the Pt substrate, the response was essentially reversible; the ratio of the

anodic and cathodic peak currents, $i_{p,a}/i_{p,c}$ was approximately 1, the peak-to-peak separation, ΔE_p was approximately 60 mV, the peak potentials, $E_{p,a}$ and $E_{p,c,}$ were independent of the scan rate, υ, and i_p was proportional to $\upsilon^{1/2}$. However, the CVs obtained at the wrought Inconel 625 substrate (Figure 2B), the Inconel 625 coating (Figure 2C) and at the stainless steel surface (Figure 2D) were all markedly different to that obtained at Pt. ΔE_p for FcOH oxidation and reduction was greater than 500 mV in each case and increased as υ increased, as expected for kinetically-controlled heterogeneous ET reactions. In the case of the stainless steel surface, the peak due to reduction of FcOH was observed at approximately -0.1 V and the peak for FcOH was observed at approximately 0.7 V. However, the oxidation peak was obscured by the presence of a large peak centred at approximately 1.1 V. Unlike the peaks due to FcOH oxidation and reduction observed at each substrate surface, i_p for this peak was proportional to υ, suggesting that it was due to a surface process. To confirm that this was a surface oxidation peak, a CV was recorded at the stainless steel surface in blank K_2SO_4 and this is shown by the dashed line in Figure 2D. The presence of this peak in the CV obtained in the blank electrolyte clearly shows that the peak was due to oxidation of the stainless steel surface.

3.3 Measuring the Kinetics of Heterogeneous Electron Transfer using SECM

The kinetics of ET across the substrate/electrolyte interface can be measured using SECM feedback approach curves obtained when the tip process is diffusion limited [28]. The rate constant for heterogeneous ET across the substrate/electrolyte

interface, k, can be obtained by fitting an experimental current-distance curve to Equation 1:

$$I_T(L) = I_S(1-I_T^{ins}/I_T^C) + I_T^{ins} \quad (1)$$

where I_T(L) is the tip current at normalised distance, L, from the substrate, I_T^C is the normalised tip current at the same L value for diffusion-controlled positive feedback at a conducting substrate:

$$I_T^C = 0.68 + 0.78377/L + 0.3315\exp(-1.0672/L) \quad (2)$$

I_S is the normalised kinetically-controlled substrate current:

$$I_S = 0.78377/L(1 + 1/\Lambda) + [(0.68 + 0.3315\exp(-1.0672/L)]/[1 + F(L,\Lambda)] \quad (3)$$

where $\Lambda = \kappa L$, $\kappa = ka/D$, a is the SECM tip radius, D is the diffusion coefficient of the redox species and $F(L,\Lambda) = (11/\Lambda + 7.3)/110 - 40L)$. I_T^{ins} is given by Equation 4:

$$I_T^{ins} = 1/(0.15 + 1.5385/L + 0.58\exp(-1.14/L) + 0.0908\exp[(L - 6.3)/(1.017L)]) \quad (4)$$

Equation 1 is valid in the range $0.01 \leq \kappa \leq 1000$ and, by fitting experimental approach curves to theoretical curves generated for various values of κ, the kinetics of electron transfer across the substrate/electrolyte interface can be measured. In this study, the Pt SECM tip was held at 0.6 V to drive the diffusion-limited oxidation of FcOH to $FcOH^+$ and a series of current-distance curves were recorded at each substrate at a range of substrate potentials [29]. For example, Figure 3A (solid lines) shows a series of experimental approach curves recorded at a stainless steel substrate as the substrate potential was systematically altered. The increase in the tip currents in each curve as the substrate potential was made more negative shows that the rate of reduction of $FcOH^+$ to FcOH at the substrate increased as the substrate potential became more negative. The open circles in Figure 3A show the best fits for each curve obtained by fitting the experimental curves to Equation 1 and, from these fits, a κ value was obtained for the substrate reaction at each substrate potential. The best-fit κ values (see Figure 3 legend) fall within the region of validity of Equation 1 ($0.01 \leq \kappa \leq 1000$) and, using this data, Tafel plots of ln k ($k = \kappa D/a$) versus the overpotential, η ($\eta = E - E^{0'}$, where $E^{0'}$ is the formal potential of the $FcOH/FcOH^+$ redox couple) were constructed. Figure 3B shows a typical Tafel plot obtained using the fits shown in Figure 3A. Good linearity was observed in the Tafel plot indicating that valid kinetic measurements could be performed at this surface using SECM. This procedure was repeated for the wrought Inconel 625 and the fitted SECM feedback approach curves and Tafel plot obtained at this surface are shown in Figure 4. Good linearity of the Tafel plot was also obtained for the data obtained at the wrought Inconel 625. Extrapolation of each Tafel plot to zero overpotential yielded k^0 values of $1.3 \pm 0.5 \times 10^{-4}$ cm s^{-1} and $7.7 \pm 0.8 \times 10^{-4}$ cm s^{-1} for the stainless steel substrate and the wrought Inconel 625 substrate,

respectively. It is important to note that the rate of ET was measured in at least 3 random locations on the surface and the error is the standard deviation of these measurements. It is also important to note that feedback-mode SECM images of the wrought Inconel surface do not reveal any features indicating that the surface of wrought Inconel 625 is electrochemically homogeneous [23]. The transfer coefficient, α, was determined from the slopes of the Tafel slopes and was 0.33 and 0.20 for the stainless steel substrate and the wrought Inconel 625, respectively, which are significantly lower than the value of approximately 0.5 expected for a simple outer-sphere ET reaction. However, these α values are close to that reported recently by Mirkin and co-workers for the $Ru(NH_3)_6^{3+/2+}$ redox couple at a stainless steel surface (α = 0.15)[14]. Notably. the k^0 values measured for FcOH reduction at stainless steel and wrought Inconel 625 are orders of magnitude lower than the k^0 values of between 0.2 and 2.0 cm s^{-1} determined using carbon and Pt electrodes [30-32]. However, the k^0 values determined here are reasonably close to that determined by Mirkin for $Ru(NH_3)_6^{3+/2+}$ at stainless steel ($\sim 10^{-3}$ cm s^{-1}). It is highly likely that, as in the case of $Ru(NH_3)_6^{3+/2+}$ oxidation at stainless steel, both k^0 and α are affected by the presence of the passive film on the substrate surface [14].

The radius of the area of the substrate that participates in the feedback loop during SECM experiments is $r \cong a + 1.5\ d$, where d is the tip-substrate separation [28]. Therefore, it is possible to perform local kinetic measurements using SECM feedback experiments. Kinetic measurements were performed at a number of locations on a thermal sprayed Inconel 625 surface by first recording a feedback-mode image of the surface, which is shown in Figure 5. The gradual increase in i_T from the top to the bottom of Figure 5 is due to a slight tilt of the substrate. However, this image shows

regions of higher and lower electrochemical activity, as was observed at thermal sprayed Inconel 625 coatings previously [23]. These regions of higher activity were approximately 50 μm in diameter, which is twice the diameter of the SECM tip used in our experiments. Therefore, based on the relative dimensions of the tip and the regions of high activity on the surface, it should be possible to perform kinetic measurements at these locations and detect differences in electrochemical activity.

Feedback approach curves were recorded at a range of substrate potentials at each of the regions labelled a-f in Figure 5 and these are shown in Figure 6, along with the best-fits to the data generated using Equation 1. Tafel plots of ln k versus η were constructed for each of the data sets obtained at the thermal sprayed surface and these are shown in Figure 7. k^0 values determined for $FcOH^+$ reduction from the Tafel plots at each location are shown in Table 1. The average k^0 value at the "inactive" sites (a, b and c) on the sprayed surface was $2.76 \pm 0.8 \times 10^{-4}$ cm s^{-1}, which was lower than that measured at the active sites d, e and f ($4.94 \pm 0.5 \times 10^{-4}$ cm s^{-1}). Therefore, the brown spots in the feedback SECM images obtained at thermally sprayed Inconel 625 surfaces clearly correspond to regions of higher electrochemical activity. It is important to note that the substrate roughness was such that topographic effects should be negligible during SECM imaging (see experimental section). Therefore, the heterogeneity in the rate of $FcOH^+$ reduction at the sprayed sample is clearly a result of the spraying process as such heterogeneity was not detected at the wrought Inconel 625 substrate. However, it is clear from our data that the spraying process does not increase the average electrochemical activity of the surface significantly beyond that of the wrought material. In fact, the average k^0 at the sprayed surface was slightly lower than that measured at the wrought alloy. Therefore, it appears that the protective oxide that forms on the

sprayed surface hinders the electrochemical activity of the surface to a similar extent to the oxide formed on the wrought superalloy. It is possible that the spraying process introduces local variations in the thickness of the oxide layer on the sprayed surface as it solidifies and it is these variations in the oxide thickness that are the source of the heterogeneity of the surface activity. It is possible that the splat boundaries are the source of this heterogeneity as de-alloyed elements can be found in these regions. We are currently exploring this concept further using surface analysis but, as our results here show, SECM is very useful for quantifying the effect of thermal spraying on the electrochemical activity of superalloys.

4. Conclusions

In this study, SECM has been used to measure the rate of electron transfer across the interface between a thermal sprayed anti-corrosion superalloy (Inconel 625) coating and an aqueous electrolyte. The rate of electron transfer from the coating to a redox species in solution was measured at discrete locations on the sprayed surface and the rate varied across the surface. This data correlated very well that obtained using SECM imaging, which suggested that the sprayed surface was electrochemically heterogeneous. In addition, the data obtained from the sprayed surface was compared with data obtained from samples of the bulk wrought superalloy and stainless steel. Our analysis reveals that, while the thermal spraying process introduces significant heterogeneity to the superalloy surface, the electrochemical activity of the coating is comparable to that of the bulk superalloy and higher than that of stainless steel. Thus,

for the first time, we have used SECM to obtain quantitative insights into the effect of thermal spraying on the electrochemical activity of corrosion-resistant superalloy coatings.

Acknowledgements

We thank the University of Nottingham Research Strategy Fund for funding. DW also thanks the EPSRC for funding this work through the Science and Innovation Award (Driving Innovation in Chemistry and Chemical Engineering: Grant EP/D501229/1)

Table 1. Standard heterogeneous electron transfer rate constants determined at the locations marked a-f in Figure 7.

Location	k^0 / cm s^{-1}
a	3.54×10^{-4}
b	2.01×10^{-4}
c	2.73×10^{-4}
d	5.23×10^{-4}
e	5.25×10^{-4}
f	4.33×10^{-4}

FIGURE LEGENDS

Figure 1. (A) SEM image of the surface of wrought Inconel 625. (B) SEM image of the surface of HVOF-sprayed Inconel 625 coatings on mild steel substrates. The black and white arrows show HVOF thermal-spray formed splats and splat boundaries, respectively. (C) High magnification image of a splat boundary.

Figure 2. Cyclic voltammograms obtained in 1mM FcOH in 0.1 M K_2SO_4 at (A) a 2 mm diameter Pt disk, (B) wrought Inconel 625 (C) an Inconel 625 coating and (D) stainless steel. All CVs were recorded at 10, 20, 30, 40 and 50 mV s^{-1} and the potential limits were (A) 0.0 to 0.6 V, (B) -0.2 to 0.6 V, (C) -0.2 to 0.6 V and (D) -0.4 to 1.2 V, respectively. The dotted line in D shows the voltammogram obtained at stainless steel in blank 0.1 M K_2SO_4 at 10 mV s^{-1}.

Figure 3. (A) Experimental SECM feedback approach curves (solid lines) obtained at a stainless steel surface using a 12.5 μm radius Pt SECM tip. The tip potential was 0.6 V and the substrate potential was (from bottom to top) 0.05, 0.0, -0.05, -0.10, -0.15, -0.20, -0.25, -0.30, -0.35 and -0.40 V vs Ag|AgCl. The open circles show the theoretical responses generated using Equation 1 with (from bottom to top) κ = 0.064, 0.112, 0.176, 0.288, 0.512, 0.849, 1.57, 2.40, 3.28 and 4.80. (B) Tafel plots of ln k versus overpotential, η, obtained using the data shown in A.

Figure 4. (A) Experimental approach curves (solid lines) obtained at a wrought Inconel 625 surface using a 12.5 μm radius Pt SECM tip. The tip potential was 0.6 V and the substrate potential was (from bottom to top) 0.10, 0.05, 0.0, -0.05, -0.10, -0.15, -0.20, and -0.25 V vs Ag|AgCl. The open circles show the theoretical responses generated using Equation 1 with (from bottom to top) κ = 0.321, 0.465, 0.673, 1.042, 1.522, 2.163, 2.965 and 3.846. (B) Tafel plots of ln k versus overpotential, η, obtained using the data shown in A.

Figure 5. SECM image obtained at a HVOF-sprayed Inconel 625 coating on mild steel by recording i_T as a 12.5 μm radius Pt SECM tip was scanned in x-y plane at 250 μm s^{-1}. The tip was held at 0.6 V to drive the oxidation of FcOH at a diffusion-controlled rate, the substrate was at open circuit potential and the tip-substrate distance was 4 μm (0.3 L). The electrolyte was 0.1 M K_2SO_4, which contained 1 mM FcOH.

Figure 6. Experimental approach curves (solid lines) obtained at HVOF-sprayed Inconel 625 coating on mild steel surface at active sites (a, b, c in Figure 5) and less active sites (d, e, f in Figure 5) using a 12.5 μm radius Pt SECM tip. The tip potential was 0.6 V and the substrate potential was (from bottom to top) 0.15, 0.10, 0.05, 0.0, -0.05, -0.10, -0.15, -0.20 and -0.25 V vs Ag|AgCl. The open circles show the theoretical responses generated using Equation 1 with (from bottom to top) κ = 0.080, 0.160, 0.256, 0.353, 0.561, 0.785, 1.089, 1.410, and 1.923 at site a, κ = 0.048, 0.144, 0.256, 0.385, 0.641, 1.042, 1.522, 2.244 and 3.045 at site b, κ = 0.080, 0.160, 0.321, 0.561,

0.962, 1.442, 2.163, 3.045 and 3.526 at site c, κ = 0.160, 0.321, 0.481, 0.881, 1.362, 2.434, 3.846, 6.410 and 10.417 at site d, κ = 0.144, 0.304, 0.513, 0.897, 1.442, 2.244, 3.205, 4.167 and 5.289 at site e and κ = 0.112, 0.256, 0.369, 0.593, 0.962, 1.442, 2.244, 3.205 and 4.167 at site f.

Figure 7. Tafel plots of ln k versus overpotential, η, obtained using the data shown in Figure 6. (A) Tafel plots for the data obtained at active sites a (Δ), b (○) and c (□). (B) Tafel plots for the data obtained at less active sites d (○), e (Δ) and f (□).

FIGURE 1

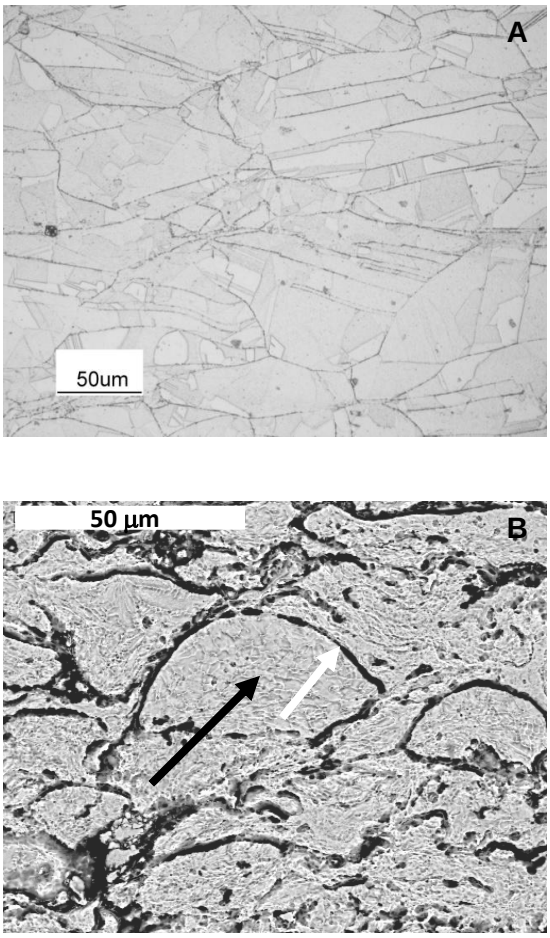

FIGURE 2

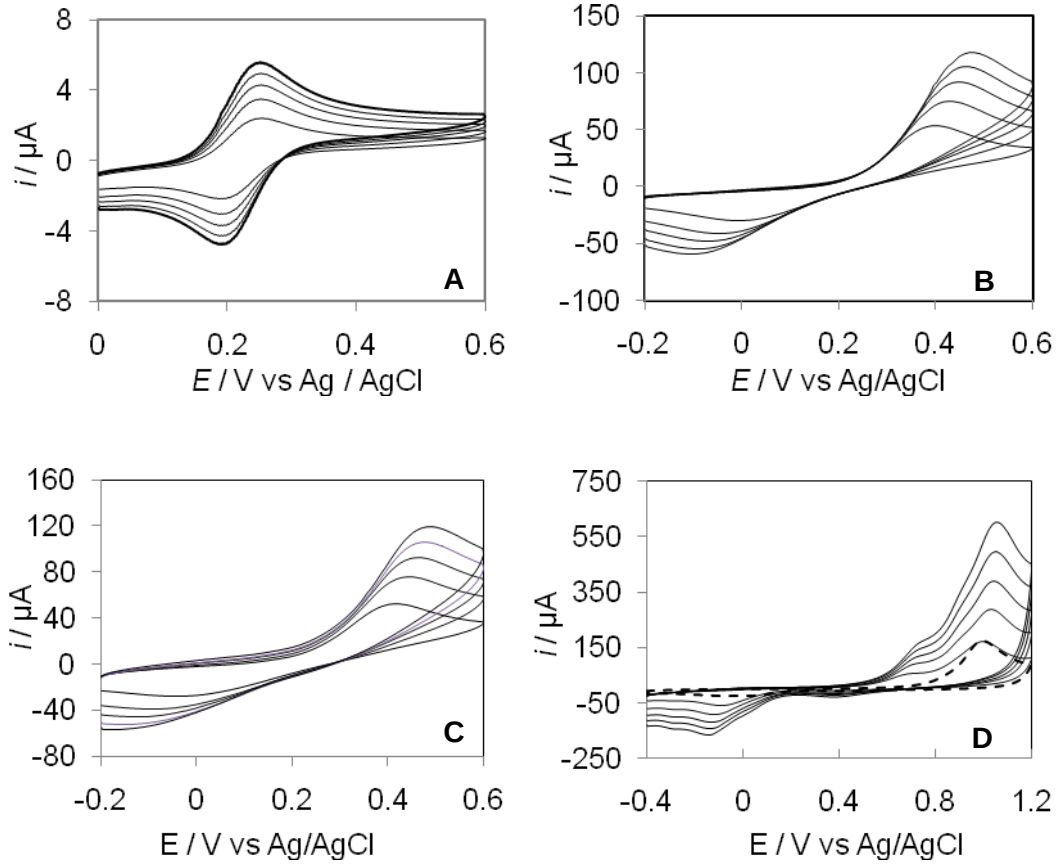
8
4
0
-4
-8
i / µA
A
0
0.2
0.4
0.6
E / V vs Ag / AgCl
150
100
50
0
-50
-100
i / µA
B
-0.2
0
0.2
0.4
0.6
E / V vs Ag/AgCl
160
120
80
40
0
-40
-80
i / µA
C
-0.2
0
0.2
0.4
0.6
E / V vs Ag/AgCl
750
550
350
150
-50
-250
i / µA
D
-0.4
0
0.4
0.8
1.2
E / V vs Ag/AgCl

FIGURE 3

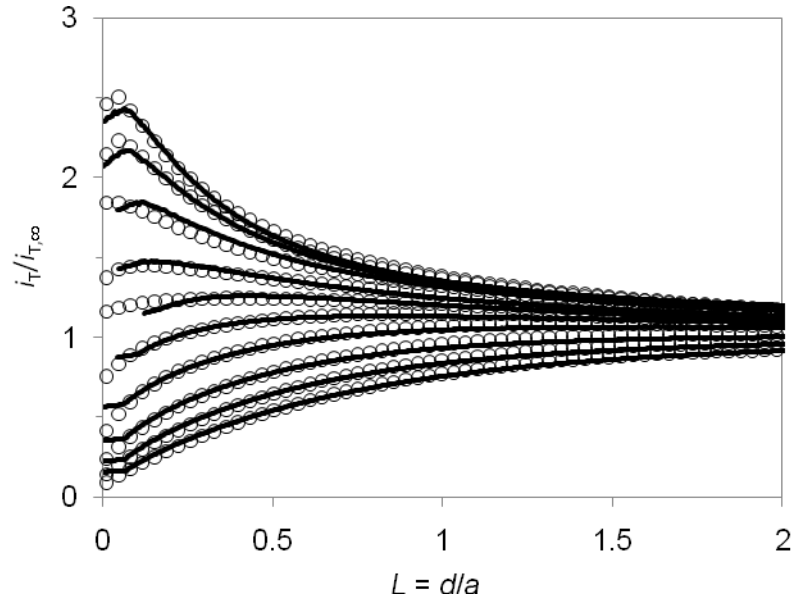
3
2
1
0
0
0.5
1
1.5
2
$i_T/i_{T,\infty}$
$L = d/a$

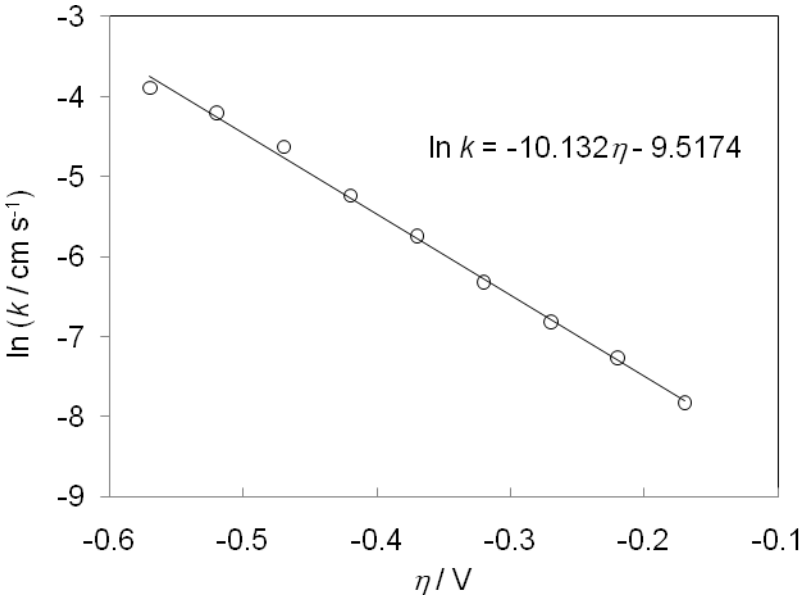
-3
-4
-5
-6
-7
-8
-9
-0.6
-0.5
-0.4
-0.3
-0.2
-0.1
ln (k / cm s^{-1})
η / V
ln k = -10.132η - 9.5174

FIGURE 4

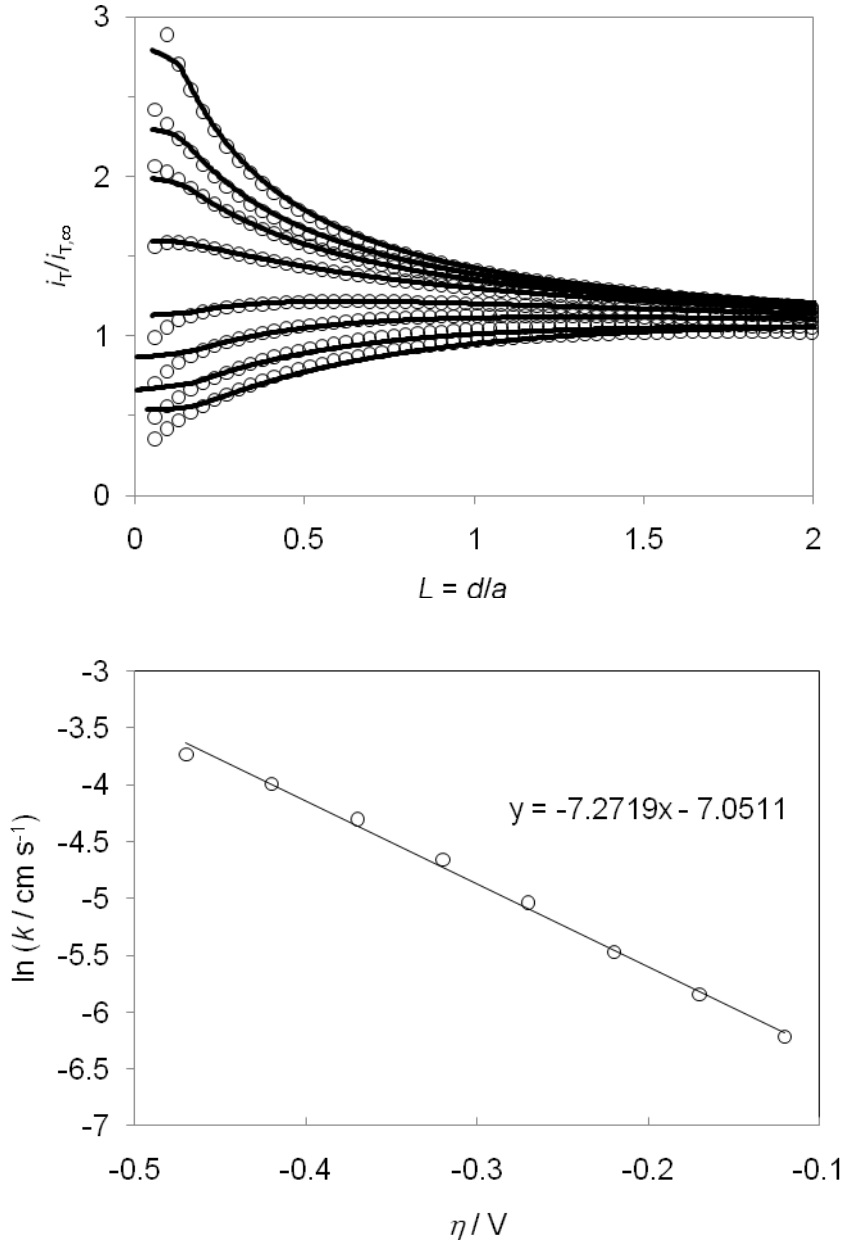
3
2
1
0
0
0.5
1
1.5
2
$i_T/i_{T,\infty}$
$L = d/a$
-3
-3.5
-4
-4.5
-5
-5.5
-6
-6.5
-7
-0.5
-0.4
-0.3
-0.2
-0.1
y = -7.2719x - 7.0511
ln (k / cm s^{-1})
η / V

FIGURE 5

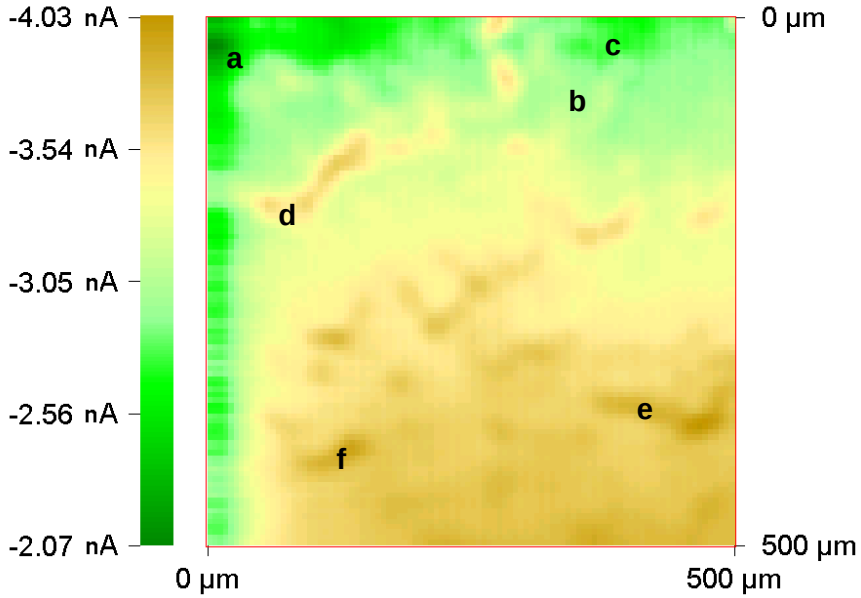

FIGURE 6

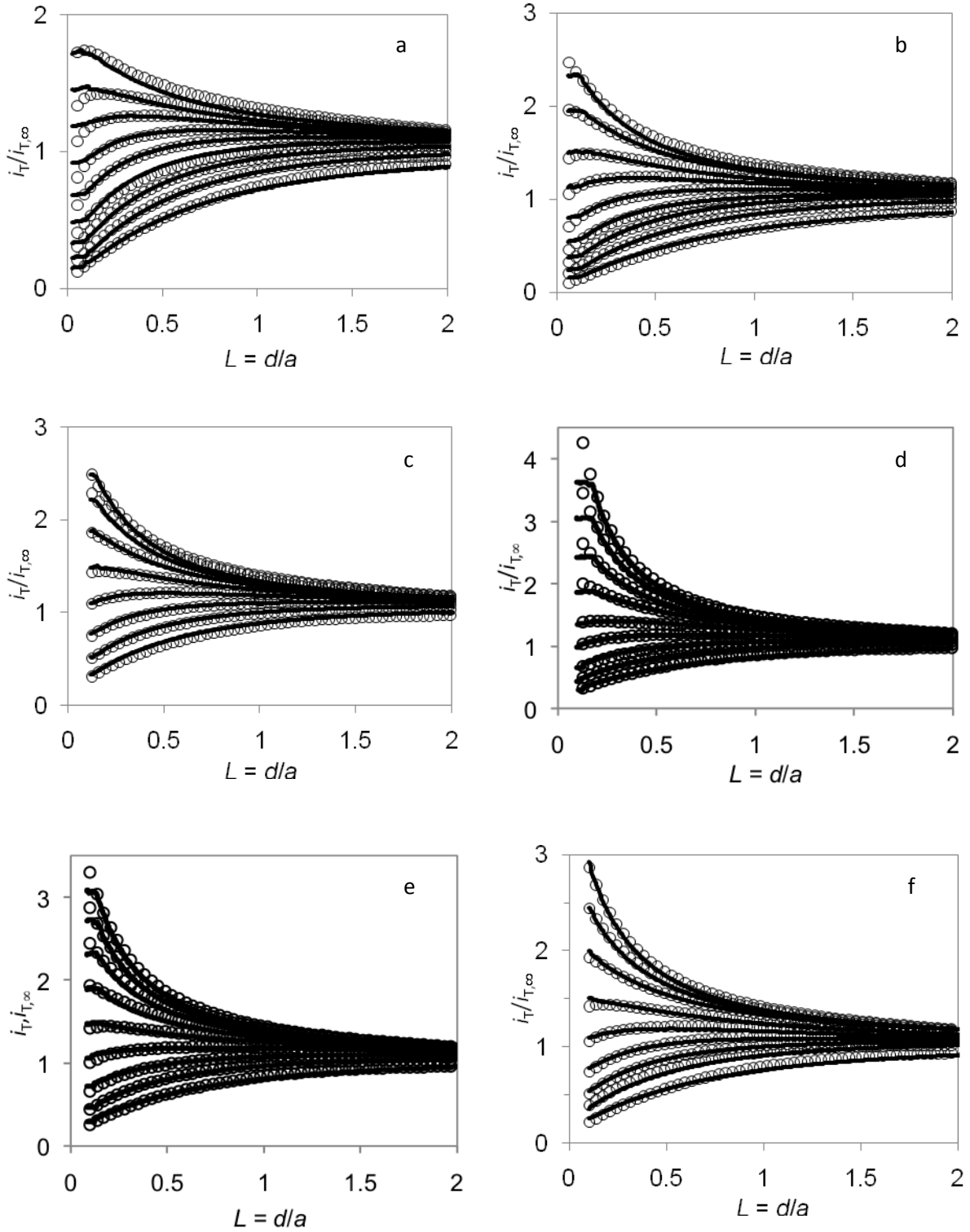

FIGURE 7

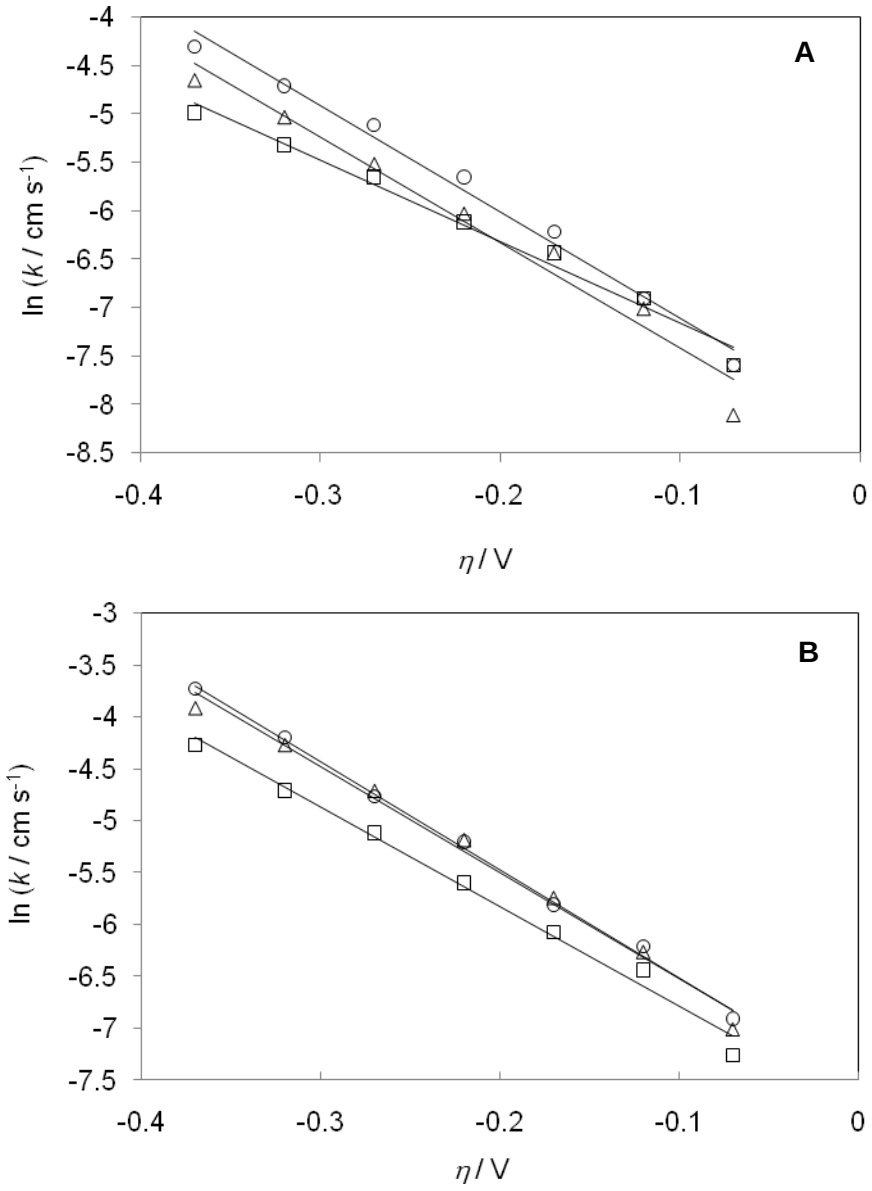

References

[1] J. R. Davis, Handbook of Thermal Spray Technology, ASM International, Materials Park, OH, USA, 2004.

[2] J. H. He, J.M. Schoenung, Mater. Sci. Eng., A, 336 (2002) 274-319.

[3] P. Fauchais, A. Vardelle, B. Dussoubs, J. Therm. Spray Technol., 10 (2001) 44-66.

[4] C. Verdon, A. Karimi, J.L. Martin, Mater. Sci. Eng. A-Struct. Mater. Prop. Microstruct. Process., 246 (1998) 11-24.

[5] D. Toma, W. Brandl, G. Marginean, Surf. Coat. Technol., 138 (2001) 149-158.

[6] A. Kulkarni, J. Gutleber, S. Sampath, A. Goland, W.B. Lindquist, H. Herman, A.J. Allen, B. Dowd, Mater. Sci. Eng. A-Struct. Mater. Prop. Microstruct. Process., 369 (2004) 124-137.

[7] E. Petrovicova, R. Knight, L.S. Schadler, T.E. Twardowski, J. Appl. Polym. Sci., 78 (2000) 2272-2289.

[8] G. Bolelli, L. Lusvarghi, R. Giovanardi, Surf. Coat. Technol., 202 (2008) 4793-4809.

[9] A.J. Sturgeon, J. Mater. Sci., 32 (1997) 863 - 872.

[10] K. Fushimi, K.A. Lill, H. Habazaki, Electrochim. Acta, 52 (2007) 4246-4253.

[11] P. Sun, F. Ois, O. Laforge, M.V. Mirkin, Phys. Chem. Chem. Phys., 9 (2006) 802–823.

[12] C. Gabrielli, S. Joiret, M. Keddam, H. Perrot, N. Portail, P. Rousseau, V. Vivier, Electrochim. Acta, 52 (2007) 7706-7714.

[13] D.O. Wipf, Colloids Surf., A, 93 (1994) 251-261.

[14] P. Sun, Z. Liu, H. Yu, M.V. Mirkin, Langmuir, 24 (2008) 9941-9944.

[15] I. Serebrennikova, H.S. White, Electrochem. Solid-State Lett., 4 (2001) B4-B6.

[16] M. B. Jensen, A. Guerard, D. E. Tallman, G. P. Bierwagenb, J. Electrochem. Soc., 155 (2008) C324-C332.

[17] J.C. Seegmiller, D.A. Buttry, J. Electrochem. Soc., 150 (2003) B413-B418.

[18] A.M. Simoes, D. Battocchi, D.E. Tallman, G.P. Bierwagen, Corros. Sci., 49 (2007) 3838-3849.

[19] A. Davoodi, J. Pan, C. Leygraf, S. Norgren, Electrochim. Acta, 52 (2007) 7697-7705.

[20] R. Zhu, C. Nowierski, Z. Ding, J.J. Noel, D.W. Shoesmith, Chem. Mater., 19 (2007) 2533-2543.

[21] S. B. Basame, H.S. White, J. Phys. Chem., 99 (1995) 16430-16435

[22] S. B. Basame, H.S. White, Anal. Chem., 71 (1999) 3166-3170

[23] D.A. Walsh, L.E. Li, M.S. Bakare, K.T. Voisey, Electrochim. Acta, 54 (2009) 4647-4654.

[24] A.J. Bard, in: A.J. Bard, M.V. Mirkin (Eds.) Scanning Electrochemical Microscopy, Marcel Dekker, New York, 2001.

[25] N. Ahmed, M.S. Bakare, D.G. McCartney, K.T. Voisey, Surf. Coat. Technol., 204 (2010) 2294-2301.

[26] V. Shankar, B.S. Rao, K. Mannan, J. Nucl. Mater., 288 (2001) 222-232.

[27] M.P. Planche, B. Normand, H. Liao, G. Rannou, C. Coddet, Surf. Coat. Technol., 157 (2002) 247-256.

[28] M.V. Mirkin, Determination of Electrode Kinetics, in: C.G. Zoski (Ed.) Handbook of Electrochemistry, Elsevier, 2007, pp. 639-660.

[29] S. Bollo, S. Finger, J.C. Sturm, L.J. Nunez-Vergara, J.A. Squella, Electrochim. Acta, 52 (2007) 4892-4898.

[30] W.J. Miao, Z.F. Ding, A.J. Bard, J. Phys. Chem. B, 106 (2002) 1392-1398.

[31] C. Bourdillon, C. Demaille, J. Moiroux, J.M. Saveant, J. Am. Chem. Soc., 117 (1995) 11499-11506.

[32] A.P. O'Mullane, J. Zhang, A. Brajter-Toth, A.M. Bond, Anal. Chem., 80 (2008) 4614-4626.